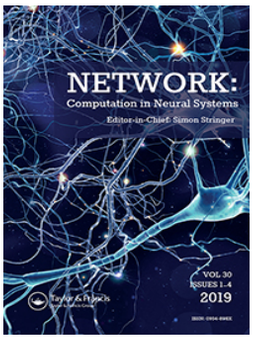

Taylor & Francis
Taylor & Francis Group

Network: Computation in Neural Systems

ISSN: 0954-898X (Print) 1361-6536 (Online) Journal homepage: www.tandfonline.com/journals/inet20

Epileptic source connectivity analysis based on estimating of dynamic time series of regions of interest

Mayadeh Kouti, Karim Ansari-Asl & Ehsan Namjoo

To cite this article: Mayadeh Kouti, Karim Ansari-Asl & Ehsan Namjoo (2019) Epileptic source connectivity analysis based on estimating of dynamic time series of regions of interest, Network: Computation in Neural Systems, 30:1-4, 1-30, DOI: 10.1080/0954898X.2019.1634290

To link to this article: https://doi.org/10.1080/0954898X.2019.1634290

NETWORK: COMPUTATION IN NEURAL SYSTEMS
2019, VOL. 30, NOS. 1–4, 1–30
https://doi.org/10.1080/0954898X.2019.1634290

Taylor & Francis
Taylor & Francis Group

ARTICLE

Epileptic source connectivity analysis based on estimating of dynamic time series of regions of interest

Mayadeh Kouti, Karim Ansari-Asl, and Ehsan Namjoo

Department of Electrical Engineering, Faculty of Engineering, Shahid Chamran University of Ahvaz, Ahvaz, Iran

ABSTRACT

We propose a new source connectivity method by focusing on estimating time courses of the regions of interest (ROIs). To this aim, it is necessary to consider the strong inherent non-stationary behavior of neural activity. We develop an iterative dynamic approach to extract a single time course for each ROI encoding the temporal non-stationary features. The proposed approach explicitly includes dynamic constraints by taking into account the evolution of the sources activities for further dynamic connectivity analysis. We simulated an epileptic network with a non-stationary structure; accordingly, EEG source reconstruction using LORETA is performed. Using the reconstructed sources, the spatially compact ROIs are selected. Then, a single time course encoding the temporal non-stationarity is extracted for each ROI. An adaptive directed transfer function (ADTF) is applied to measure the information flow of underlying brain networks. Obtained results demonstrate that the contributed approach is more efficient to estimate the ROI time series and ROI to ROI information flow in comparison with existing methods. Our work is validated in three drug-resistance epilepsy patients. The proposed ROI time series estimation directly affects the quality of connectivity analysis, leading to the best possible seizure onset zone (SOZ) localization verified by electrocorticography and post-operational results.

ARTICLE HISTORY
Received 23 August 2018
Revised 30 April 2019
Accepted 17 June 2019

KEYWORDS
Source connectivity analysis; region of interest (ROI); EEG source imaging; panelized least square; non-stationary neural activity; epilepsy

Introduction

Recently, neuroimaging techniques have been widely used to identify brain networks and interactions between brain areas (Schoffelen and Gross 2009). Among different modalities, electrophysiological measures such as electroencephalography (EEG) and magnetoencephalography (MEG) have excellent temporal resolution and can provide proper insight into the connectivity networks between anatomical regions (Da Silva 2013; Leistritz et al. 2016).

In many studies connectivity measures have been applied to the sensor level; but, interpretation of extracted connectivity at the M/EEG sensor level is not

CONTACT Karim Ansari-Asl karim.ansari@scu.ac.ir Department of Electrical EngineeringFaculty of Engineering, Shahid Chamran University of Ahvaz, Ahvaz, Iran

direct, because these recordings have a limited spatial resolution and are degraded by volume conduction effect (Haufe et al. 2013; Toppi et al. 2016).

To address this problem, some methods perform the connectivity analysis among brain sources which are estimated from M/EEG recordings (Brookes et al. 2014; Hassan et al. 2014, 2017; Sohrabpour et al. 2016; Martinez-Vargas et al. 2017; Rajabioun et al. 2017; Staljanssens et al. 2017; Ghumare et al. 2018; Hassan and Wendling 2018; He et al. 2018a). M/EEG source imaging is the technique of projecting M/EEG data to cortical source space, where generally, a realistic model of the brain cortex represents as the cortical source space (He et al. 2011, 2018a, 2018b).

Popular approaches for source modeling such as weighted minimum-norm estimate (MNE) (Hämäläinen and Ilmoniemi 1994), weighted MNE (WMNE) (Dale and Sereno 1993), Low-Resolution Tomography (LORETA) (Pascual-Marqui et al. 1994) and standardized low-resolution brain electromagnetic tomography (sLORETA) (Pascual-Marqui 2002) are based on minimizing L_2 norm. MNE minimizes the whole power of the sources and generally yields smooth source distributions (Hämäläinen and Ilmoniemi 1994). However, MNE is biased towards superficial sources. To alleviate this drawback, WMNE uses the columns norm of the lead field matrix in order to weight the regularization term. In other word, superficial sources are penalized more than the deep ones, since the deep sources do not demonstrate well in the scalp potential (Dale and Sereno 1993)]. Basically, the popular LORETA method is a WMN solution where the weighting matrix is a discrete Laplacian operator L (the second-order spatial derivatives of the sources), leads to explicitly promoted spatial smoothness (Pascual-Marqui et al. 1994). sLORETA standardizes reconstructs the sources with respect to the variance of the sources and is robust against noise and superficial sources (Pascual-Marqui 2002). These methods are commonly used to investigating EEG-based connectivity between sources (Hassan et al. 2014, 2017; Sohrabpour et al. 2016; Wang et al. 2016; Mahjoory et al. 2017; Staljanssens et al. 2017; Hassan and Wendling 2018).

After sources reconstruction, the connectivity analysis between the reconstructed sources can be performed by using an extensive variety of techniques such as Granger causality (GC) (Kaminski and Blinowska 1991; Astolfi et al. 2006; Valdes-Sosa et al. 2011), phase synchronization (Campbell et al. 1980) or cross-spectrum (Nunez et al. 1997; Nolte et al. 2004; Chella et al. 2014) among the source reconstructed time series (Astolfi et al. 2006; Hassan et al. 2014, 2017; Sohrabpour et al. 2016; Mahjoory et al. 2017). Results of all these methods are highly related to the accuracy of the selected sources time courses. For smoothly distributed sources, estimated source activities spread over the whole cortical mesh. Therefore, extracting the representative time series may not show a sufficient degree of accuracy. On the other hand, Regions of Interest (ROIs) and their corresponding time series are known to have an important impact on the accurate estimate of the connectivity measure (Mahjoory et al. 2017; Ghumare et al. 2018; Hassan and Wendling 2018).

There are two different strategies to define ROIs. The first one, named pre-defined ROI identification, can be achieved based on some prior information about ROIs association in experimental tasks (Astolfi et al. 2004), or by tracking the structural connectivity networks (Pineda-Pardo et al. 2014). In the second strategy, no pre-defined ROI is expected and the entire process of finding network points and extracting time series for each node is completely data driven. A widely common non pre-defined ROIs identification strategy is to determine strong reconstructed areas during the experimental tasks.

In this paper, similar to (Friston et al. 2008), we use a non-identified ROI selection strategy by developing a data-driven method to assigned ROIs within small clusters. The proposed strategy uses the neighboring information of the Green's function $\mathbf{Q}_G$ (Friston et al. 2008) to select the spatial ROI location precisely. Connectivity estimation between all ROIs depends on the ROI time courses quality. Computing connectivity among all the dipoles belonging to the ROIs increases the computational complexity. The most common way is to average the ROI time series through all the specific ROI sources (Hassan and Wendling 2018). Since the ROIs may encompass dipoles with different dynamics, time course averaging leads to an additional blurred result. In addition to average ROI time series an alternative method is extracting the time courses from the most powerful dipole (Courellis et al. 2017); however, this strategy does not correctly comprise the temporal dynamic of the entire region. In (Sohrabpour et al. 2016), the time series of the dipole with the maximum singular value in the region is selected as ROI time series. In (Farahibozorg et al. 2018), the dipole that shows the maximum cross-talk function (CTF) index in each ROI is used. In similar works (Hauk et al. 2011; Stenroos and Hauk 2013), the dipole that displays the resolution index closest to 1 in the region is employed. Recently, the dipole with the maximum correlation with the averaged time series of all dipoles within the region is selected to show each ROI time course (Ghumare et al. 2018).

This work proposes an approach to estimate the dynamics of every ROI in such a way that a single time course contains the time variation of each certain region (Martinez-Vargas et al. 2017). To aim this goal, the brain activities are forced to come out only inside the regions of interest. Then, the ROI time series are estimated through a temporal penalty in the cost function that makes the temporal solution be constant within a temporal neighborhood but vary during an extended time period, *i.e.*, local stationary. This term improves the time series estimation by following non-stationary activities of EEG data.

Once time series are extracted for selected dipoles using the proposed method, the connectivity analysis is performed on these time courses, in this situation, the low spatial resolution of the EEG recordings and the volume conduction effect are improved. In this article, the performance of the connectivity measure is compared through different ROI time series estimation. Therefore, we study time-varying effective connectivity between these

selected sources to evaluate the effect of each strategy on connectivity analysis. To this end, an adaptive directed transfer function (ADTF) (Schlögl 2000; Omidvarnia et al. 2011) is computed between pairs of ROIs.

To compare different strategies, we simulate non-stationary synthetic EEG data of epilepsy onset sources with a time-varying connectivity structure; these data are generated with different SNR levels and different amount of electrode numbers are used.

The performance of the methods is evaluated by measuring the MSE (Mean Square Error) and the correlation coefficients between the time series of ground truth and estimated ROIs time series. Also, MSE of the estimated and true time-varying connectivity values is used to determine how well the ROI time series and their underlying networks can be determined. Lastly, we objectively estimate the network driver location and calculate the mean Euclidean distance between the estimated network driver zone and its ground truth. Obtained results showed that the proposed methodology has a more precise estimate of the time course of a region of interest and demonstrates more accurate network reconstruction for connectivity metrics.

Next to simulations, our work is validated in three epilepsy patients. We apply the proposed approach to find the seizure onset zone (SOZ) primarily based on time-varying effective connectivity of the estimated ROI time series. The proposed ROI time series estimation directly affects the quality of connectivity analysis, leading to the best possible SOZ localization. Validation is done by comparing the estimated SOZ with referencing region which is recognized as the s placement of the epileptogenic region and verified by electrocorticography (ECoG) and post-operational results (Zwoliński et al. 2010).

The rest of the paper is organized as follows. Methods describes methods consisting of ROI identification as well as the proposed method for extraction ROI time courses. The simulation of the epileptic network is explained in details in Simulations. Also, the proposed method is investigated in real epilepsy dataset in Real Epilepsy Dataset. In Discussion, we discuss the properties of the proposed method and results. Finally, the paper is concluded in Conclusion.

Methods

In this section, a background of source modelling is provided and then the ROI identification approach is described using spatial basis functions. Next, we formulate the recursive inverse problem solver algorithm as an ROI time series estimator.

Cortical sources mapping

To evaluate the connectivity analysis between brain regions, EEG data are projected to the source space using an inverse problem method. With this

aim, a multivariate linear model with a distributed source representation is used to express the EEG recordings:

$$Y = \boldsymbol{G}\boldsymbol{X} + \boldsymbol{\varepsilon} \tag{1}$$

where $\boldsymbol{Y} \in \mathbb{R}^{M\times T}$ is the EEG data recordings M sensors and T time samples, $\boldsymbol{X} \in \mathbb{R}^{N\times T}$ is the amplitude of N sources, and finally $\boldsymbol{G} \in \mathbb{R}^{M\times N}$ is lead field matrix presenting relationships between sources and EEG recordings contaminated with a zero mean Gaussian noise $\boldsymbol{\varepsilon} \in \mathbb{R}^{M\times T}$. For solving inverse problem, the orientation of the sources is assumed to be fixed and perpendicular to the cortical surface [33]. In this article, we use LORETA for solving inverse problem which is a minimum norm estimator.

Identification of regions of interest (ROIs)

After source reconstruction, we develop a data-driven strategy to choose the spatial ROI location and build the label matrix $\boldsymbol{\Phi}_K \in \mathrm{N}^{N\times \mathrm{K}}$ where K is the number of extracted ROIs (k-th column of the matrix $\boldsymbol{\Phi}_K$, denoted as $\boldsymbol{\varphi}_k \in \mathrm{N}^{N\times 1}$, indicates the membership of each dipole to k -th detected ROI). At first, we compute the power of brain activity from the reconstruction stage. Then, the power of all sources is scanned over the surface of the brain to find the set of the most powerful dipoles (as an effective indicator of each ROI). Consequently, we use the neighboring information of the Green's function $\boldsymbol{Q}_G = exp(\rho\boldsymbol{\Delta})$, with $\boldsymbol{Q}_G \epsilon \mathbb{R}^{N\times N}$, to select the neighborhood of each powerful dipole. $\boldsymbol{\Delta} \in [01]^{N\times N}$ is the graph Laplacian that represents connectivity information of adjacent dipoles and is calculated using a head model; this model encompasses the adjacency matrix that includes all needed cortical information (Friston et al. 2008). Besides, the constant $\rho \in \mathbb{R}^{+}$ stands for the smoothness of spatial extent of the activated areas. By using the Green's function to select regions of interest, biasing of the ROI estimates is avoided.

In practice, the ROI identification is done as follows. First, we select all sources that their powers pass a pre-defined threshold (here 10% of the amplitude of source activity with the highest power). The removed dipoles are not considered as members of any ROI. Secondly, we take the first ROI as the spatial area that is placed at the dipole location with the highest power and surrounded by using a Green function with radius ρ . All these dipoles are labeled as the first ROI. Similarly, the second ROI the dipole with the next highest power is centered, rejecting the dipoles that have been previously labeled. We repeat this procedure until the entire set of the most dominant dipoles is selected and labeled, guaranteeing that each of the most dominant dipoles belongs to a single ROI. By varying the radius ρ, number of ROIs can be changed. If the radius is too small, all sources will be selected; in

addition to high computational load, this case may bias the connectivity estimate. On the other hand, if the radius is too large, some plausible network nodes may be excluded. Therefore, the radius should be set to a value that leads a good correspondence between the LORETA solution and the selected sources. Empirically, we eventually opted for a radius of 0.6 as it provides the best result.

ROI time courses estimation

After identification of ROIs, a label has been allocated to each dipole that exceeds the prefixed threshold. However, the time series obtained from the ROI set affect highly the performance of the connectivity analysis. We addressed this issue by developing an extension of the Iterative Regularized Algorithm proposed in (Giraldo-Suarez et al. 2016) that contains spatiotemporal constraints using a spatial basis decomposition. The proposed method extracts a single time course for each ROI, considering the non-stationarity of brain activity. In this method, the source current density is modeled as a linear combination of the ROI activations as follows (Haufe et al. 2011):

$$\boldsymbol{X} = \boldsymbol{\Phi}_K \boldsymbol{C} \tag{2}$$

where $C \in \mathbb{R}^{K \times T}$ denotes the coefficients that generate the temporal dynamics of each ROI. The k -th row of C shows the time courses of the respective k -th ROI. Therefore, an estimate of C is gained by minimizing the following cost function:

$$\widehat{\boldsymbol{C}} = \arg\min_{\boldsymbol{C}} \left\{ ||\boldsymbol{Y} - \boldsymbol{G}\boldsymbol{\Phi}_K \boldsymbol{C}||_F^2 + \boldsymbol{\Theta}(\boldsymbol{C}, \lambda) \right\} \tag{3}$$

where the term $\boldsymbol{\Theta}(\boldsymbol{C}, \boldsymbol{\lambda})$ shows the constraints imposed on the regularization parameter λ and $\boldsymbol{Q}_\varepsilon \in \mathbb{R}^{\mathrm{M} \times \mathrm{M}}$ is associated to the measurement noise covariance matrix. To improve the estimate of connectivity measures, we enhance the temporal resolution of estimated ROI time series by assuming that the ROI time series are active and temporally homogeneous. To this aim, we penalize the difference between sequential time samples in the second term as follows:

$$F(\boldsymbol{c}_t, \lambda_t) = ||\boldsymbol{y}_t - \boldsymbol{G}\boldsymbol{\Phi}\boldsymbol{c}_t||_{2,\boldsymbol{Q}_\varepsilon}^2 + \lambda_{\mathrm{t}} ||\boldsymbol{c}_t - \widehat{\boldsymbol{c}}_{t-1}||_{2,\boldsymbol{Q}_\eta}^2 \tag{4}$$

where $\widehat{\boldsymbol{c}}_t$ shows the estimate of $\boldsymbol{c}_t$ at time instant t. Minimizing the regularized cost function depends on the second term in Equation (4) which is the residual norm of $\boldsymbol{c}_t$ weighted by its noise covariance matrix $\boldsymbol{Q}_\eta \in \mathbb{R}^{\mathrm{N} \times \mathrm{N}}$. This term guarantees that the estimated time courses remains almost invariant within a temporal neighborhood, but it changes over a large time period. For simplicity, both covariance matrices are assumed to be the identity matrices, *i.e.*, $\boldsymbol{Q}_\varepsilon = \boldsymbol{I}_M$ and $\boldsymbol{Q}_\eta = \boldsymbol{I}_N$. For each t, the

estimation of an ROI activity vector $\widehat{\boldsymbol{c}}_t$ is achieved by applying the Jacobian to Equation (4) with respect to the ROI activity $\boldsymbol{c}_t$ as given in Equation 5 (Giraldo-Suarez et al. 2016):

$$\frac{\partial F}{\partial \boldsymbol{c}_t} = -\boldsymbol{\Phi}^T \boldsymbol{G}^T \boldsymbol{y}_t + \boldsymbol{\Phi}^T \boldsymbol{G}^T \boldsymbol{G} \boldsymbol{\Phi} \boldsymbol{c}_t + \lambda_t \boldsymbol{c}_t - \lambda_t \widehat{\boldsymbol{c}}_{t-1} \tag{5}$$

by equaling Equation (5) to zero, accordingly, $\widehat{\boldsymbol{c}}_t$ is obtained:

$$\widehat{\boldsymbol{c}}_t = \left(\boldsymbol{\Phi}^T \boldsymbol{G}^T \boldsymbol{G} \boldsymbol{\Phi} + \lambda_t \boldsymbol{I}_K\right)^{-1} \left(\boldsymbol{\Phi}^T \boldsymbol{G}^T \boldsymbol{y}_t + \lambda_t \widehat{\boldsymbol{c}}_{t-1}\right) \tag{6}$$

Another issue to be considered is to find a proper value for the regularization parameter, λ_t, which strongly affects the estimated value of the neural activity. λ_t is calculated using General Cross-Validation (GCV) as proposed in (Grech et al. 2008):

$$\nu(\lambda_t) = \frac{||\boldsymbol{G}_N \boldsymbol{c}_t(\lambda_t) - \boldsymbol{y}_t||_2^2}{tr\left(\boldsymbol{I}_p - \boldsymbol{G}_K \boldsymbol{G}^{\dagger}(\lambda_t)\right)^2} \tag{7}$$

where $tr(.)$ indicates the sum of diagonal elements of a matrix. $\boldsymbol{G}_K = \boldsymbol{G}\boldsymbol{\Phi}$ and $\boldsymbol{G}^{\dagger}$ is the regularized inverse of the matrix $\boldsymbol{G}_K$:

$$\boldsymbol{G}^{\dagger} = \left(\boldsymbol{G}_K{}^T \boldsymbol{G}_K + \lambda_t \boldsymbol{I}_K\right)^{-1} \boldsymbol{G}_K{}^T \tag{8}$$

Time-varying effective connectivity

Once the ROI time courses are estimated, the time-varying directed connectivity between ROIs can be investigated to show information flow in the brain (Hassan et al. 2014, 2017; Leistritz et al. 2016; Sohrabpour et al. 2016) (Theiler et al. 1992; Palus and Hoyer 1998; Ding et al. 2007; Lu et al. 2012; Lie and van Mierlo 2017; Mahjoory et al. 2017; Staljanssens et al. 2017; Hassan and Wendling 2018). In this article, time-varying effective connectivity is derived using adaptive directed transfer function (ADTF) that is one of the most commonly applied Granger-based measures in the frequency domain (Schlögl 2000; Omidvarnia et al. 2011). It is designed to handle the non-stationary behavior of signals using time varying multivariate autoregressive modeling (TVAR). To this aim, at first, the ROI time courses are modeled with a TVAR model in which signals are defined as a linear combination of their past samples and an uncorrelated white noise:

$$\boldsymbol{c}_t = \sum_{p=1}^{P} A_{pt} . \boldsymbol{c}_{t-p} + \boldsymbol{e}_t \tag{9}$$

where P is the order of the model, $A_{pt} \in \mathbb{R}^{K \times K}$ is the coefficient matrix for delay p at time instant t, and $\boldsymbol{e}_t \in \mathbb{R}^{K \times 1}$ shows the uncorrelated white noise at

the same time instant. The model coefficients are estimated through a method given in (Omidvarnia et al. 2011). The Fourier transformation of the coefficient matrix is computed as follows:

$$\boldsymbol{A}(t,f) = \boldsymbol{I} - \sum_{p=1}^{P} \boldsymbol{A}_{pt} e^{-i2\pi f} \tag{10}$$

Now, the adaptive version of DTF is defined as Equation (11):

$$ADTF_{i,j}(t,f) = \frac{H_{i,j}(t,f)}{\sqrt{\sum_{j=1}^{K} \left|H_{i,j}(t,f)\right|^2}} \tag{11}$$

where $\boldsymbol{H}(t,f) = \boldsymbol{A}(t,f)^{-1}$ is time varying transfer matrix and $\boldsymbol{H}_{i,j}(t,f)$ is the entry located in the i -th row and j -th column of the matrix $H(t,f)$ that represents the information flow from the ROIs j to i, at frequency f and time instant t.

Synthetic EEG data generation

A non-stationary epileptic network, including three nodes, is simulated based on the model proposed in (Van Mierlo et al. 2011). To model an onset of the epileptogenic activity, a sinusoid function of declining frequency content from 12 Hz to 8 Hz during three seconds is employed. The seizure is originated in the first node and then propagated to the second and third nodes with 20 and 32ms delay, respectively. The sampling rate is assumed to be 250 Hz. Every active dipole belongs to a patch in the brain. Patches are in different sizes which are constructed by growing a region on the cortex using nearest neighboring elements around a randomly chosen node. In practice, a smooth activity distribution is observed due to the synchronization of neighboring neurons. The source current amplitudes in the patches are smoothed to have a Gaussian-shaped power distribution avoiding sudden power level variations. For each repetition of the experiment, all sources appear in random (surface or deeper) locations of the cortex. Also, source orientations are assumed to be fixed and orthogonal to the cortical surface [48].

To obtain more realistic simulations, both biological and measurement noises are considered. The biological noise is modeled so that it has the power spectral density inversely proportional to the frequency (also referred to as flicker or pink noise).). Moreover, a Gaussian noise is added with an SNR of 10 dB as background brain activity to 1000 randomly selected dipoles for each trial. A sample of the synthetic signals for three epileptic sources can be seen in Figure 1(a).

The cortex model is derived from an MRI atlas, namely the ICBM152 template anatomy (Mazziotta et al. 1995; Fonov et al. 2011). The atlas is divided into three layers, namely brain, skull, and skin using the FieldTrip toolbox (Oostenveld et al. 2011). A BEM model (Mosher et al. 1999)

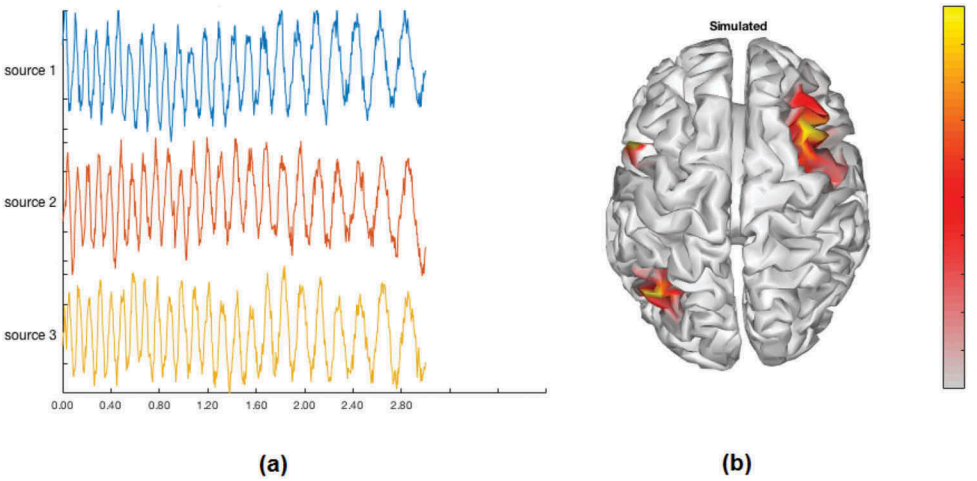

Figure 1. (a): Synthetic signals of three epileptic sources. (b): Simulated three patch sources in different sizes when SNR is 15 dB.

containing these three layers, with conductivities of 0.33 S/m, 0.0165 S/m and 0.33 S/m, is constructed to solve the forward problem. This model is used to produce the lead field matrix (Oostendorp et al. 2000; Lai et al. 2005; Zhang et al. 2006). A mesh of 5mm mean distance between adjacent vertices and consisting of 8000 nodes is used for solving inverse problem.

To obtain EEG trials with 128 channels according to the standard BIOSEMI-128 channels EEG system, the brain activity in the source domain is projected to sensor domain using lead field and source activity matrices. Additionally, a subset of 32 electrodes is selected to be tested in these simulation studies. Also, white Gaussian noise is added as the measurement noise. Another scenario to evaluate is the effect of noise on the reconstruction accuracy. We add measurement noise to consider the following values of SNR: −5, 0, 5, 10 and 15 dB. For every SNR value, each testing set includes 100 trials of simulated epileptic sources that are randomly placed on the cortex.

The errors of estimated ROI time courses and time-varying connectivity values are computed for these simulations to determine how well the ROI time series and the underlying networks can be estimated.

Simulations

As mentioned before, LORETA is used to project sensor recordings to sources in the cortex space (see Figure 2). From the reconstructed neural activity, spatially compacted ROIs sets are created using the neighboring information via the Green's function. Also, the Green function links patch points from a central point to its neighbors based on the smoothness parameter ρ. Here, to achieve a proper trade-off between local coherence and spatial accuracy the value of ρ is set

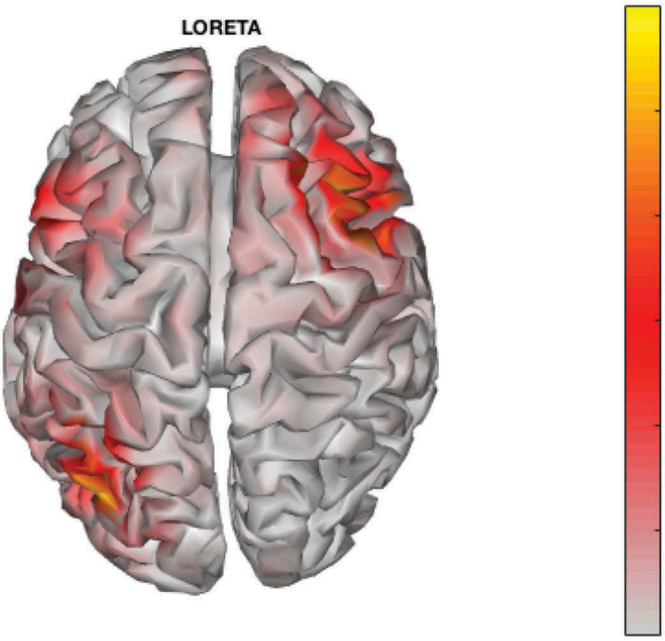

Figure 2. Reconstructed sources using LORETA. The map shows the spatial distribution of the estimated activities when SNR is 15 dB.

to 0.6. Figure 3 displays the ROI sets of the activated cortical sources; there is a strong correspondence between the true source locations (Figure 1) and their estimates (Figure 3) regardless of the considerable amount of noise.

We compare the proposed strategy (S_1) with four well-established ROI time series estimation strategies, *i.e.*, time courses of the dipole with the maximum power in the ROI (S_2) (Courellis et al. 2017), time series of the dipole with the highest singular value in the ROI (S_3) (Sohrabpour et al. 2016), time series of the dipole with the highest correlation with the averaged time series of the ROI (S_4) (Ghumare et al. 2018), the average of the estimated brain activity over the time courses of each ROI (S_5) (Hassan et al. 2014), and time course of the dipole with the nearest-to-one resolution index in the ROI (S_6) (Hauk et al. 2011; Stenroos and Hauk 2013). In the last strategy, the resolution matrix is defined as the product of the inverse kernel and the lead field matrix. Due to the ill-posed nature of the inverse problem, the resolution matrix is not an identity matrix which is the ideal situation occurs when sources are perfectly separated. To evaluate the performance of the different ROI time series estimation strategies, we use different measures:

(i) Mean squared error (MSE) between the estimated time series of ROIs and their ground truth. A lower MSE value shows better performance in recovering the time series of ROIs.

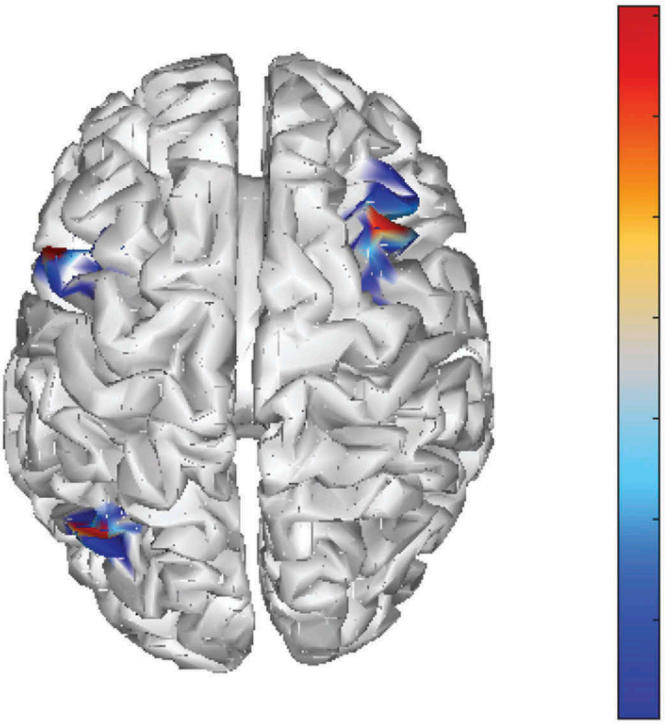

Figure 3. ROI sets of the activated cortical sources. It shows the identified spatial neighboring regions when SNR is 15 dB.

(ii) Pearson correlation coefficient between the true and extracted ROIs time series.

(iii) MSE between the theoretical and estimated ADTF parameters, which is defined as:

$$MSE_{ADTF} = \mathrm{E}[(\left|ADTF_{i,j}(t,f)\right|^2_{estimated} - \left(\left|ADTF_{i,j}(t,f)\right|^2_{groundtruth}\right)^2] \quad (12)$$

(iv) Euclidean distance between the position of the estimated seizure onset zone (SOZ) and its ground truth.

To estimate SOZ, outdegrees of all ROIs are computed and the ROI with the maximum outdegree is chosen as the SOZ. The oudegree measures the amount of outflow information from one ROI to all other ROIs. Here, the outdegree of each ROI is defined as the sum of the integrated ADTF (iADTF) parameters to all other ROIs over time (Wilke et al. 2008, 2009; van Mierlo et al. 2018). iADTF is normalization of the ADTF over the considered frequency band and its values lie within the interval $[0, 1]$. iADTF and outdegree ω_j for jth ROI are defined as below:

$$iADTF_{kj}(t) = \frac{1}{f_2 - f_1} \sum_{f=f_1}^{f_2} |ADTF_{kj}(t,f)|^2 \tag{13}$$

$$\omega_j = \sum_{k=1}^{K} \sum_{t=t_1}^{t_2} iADTF_{kj}(t) \tag{14}$$

where t_1 is the temporal seizure onset and t_2 is the temporal seizure end; and K is the number of ROIs and $iADTF_{kj}$ is the connection from ROI j to ROI k. Finally, the driver of the epileptic network (SOZ) is obtained as the ROI with the highest outdegree.

Extracting ROI time series

Figure 4(a,b) demonstrate the mean and standard error of the MSE between the estimated time series of ROIs and their ground truth after 100 trials for different SNR values for 128 and 32 electrodes, respectively. Compared to the other approaches, S_1 shows the lowest error, because the proposed methodology incorporates the brain activity dynamics into the calculation of ROIs time courses. The MSE is improved in higher levels of SNR. S_4 (based on correlation with averaged time series) and S_3 (SVD-based selection) display acceptable results; thus, they could make proper alternatives for the proposed method. On the other hand, the strategies based on the resolution index (S_6) and average over the time courses (S_5) show the worst performance. It worth mentioning that for the 32-electrode cap, similar results are observed compared to the results of the 128-electrode system. The performance of the localization method increases with the number of electrodes, corresponding to the literature (Michel and Murray 2012). In this work, it is observed that when 32 electrodes are involved, more spurious activity is appeared, which leads to higher MSE values (see Figure 4(b)).

Figure 5 shows the mean and standard error of the correlation coefficients for 100 trials of each SNR value and in both EEG channel set ups. The correlation coefficients measure the similarity of the estimated ROI time series with the ground truth. Looking at the correlation coefficients between the estimated and the ground truth time courses in Figure 5(a,b), it is clear that the dynamic ROI time series estimation (S_1) shows the highest correlation. Based on the overall results for all ROIs, we observe similar performances of almost all strategies for higher SNRs. Results given by S_4 and S_3 can be considered as second and third best method. Also, by increasing SNR and number of electrodes, improvements in correlation coefficient values are obtained.

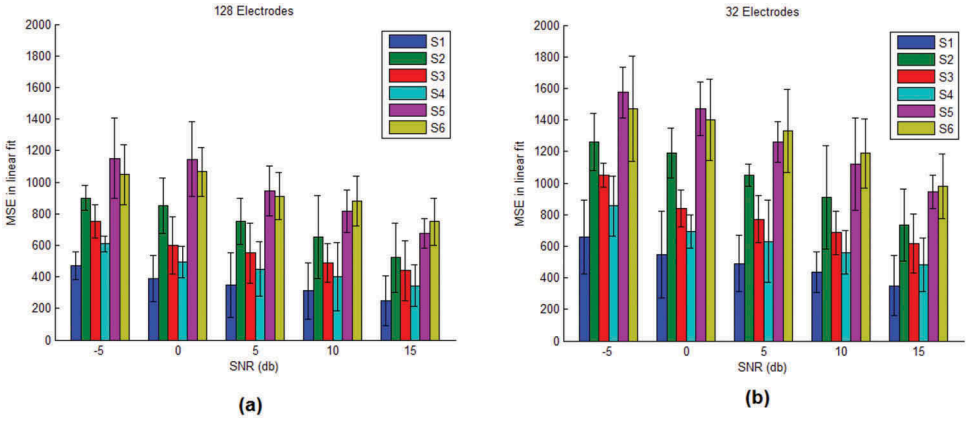

Figure 4. Performance of computer simulation; created with a BEM forward model. 100 repetitions are run with the simulated activity of three patch sources in different sizes. Each source includes non-stationary temporal dynamics of epileptic activities; see an example in Figure 1(a). Errorbars show the mean value and standard deviation of MSE between the estimated and the ground-truth time series for different ROI time series estimation strategies under several SNR levels (−5, 0, 5, 10 and 15) for 128-electrode EEG (a) and 32-electrode EEG (b) .

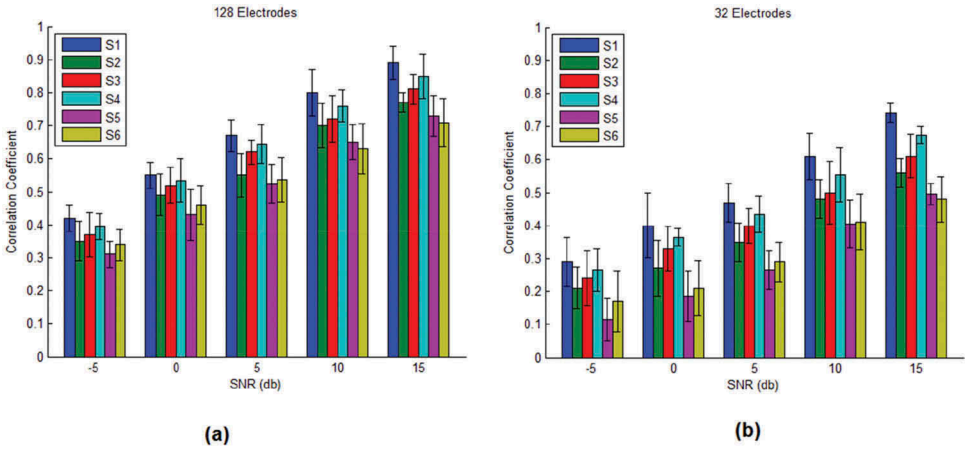

Figure 5. Performance of computer simulation; created with a BEM forward model. 100 repetitions are run with the simulated activity of three patch sources in different sizes. Each source includes non-stationary temporal dynamics of epileptic activities; see an example in Figure 1(a). Errorbars show the mean value and standard deviation of correlation coefficients between the estimated and the ground truth time series for different time series extraction strategies under several SNR levels for 128- electrode EEG (a) and 32-electrode EEG (b) .

Connectivity estimation

After the estimation of sources through the aforementioned methods, connectivity measure is done at different SNR levels and electrode numbers. ADTF is computed from the TVAR coefficients (order 5) and the frequency band of 0–30 Hz. The figures of merit are displayed for ADTF values

indicating the quality of the obtained time-varying connectivity between estimated ROI time series. The results of mean squared error after 100 trials for each SNR value are displayed in Figure 6. For 128-electrode cap (Figure 6(a)) it can be seen that the proposed strategy displays noticeable superiority in performance; because the proposed methodology incorporates the brain activity dynamics. Improvement in the performance of all strategies with increasing SNR is observed consistently. However, based on the average value of the MSE, we can see that S_1, S_4, and S_3 are superior to S_2, S_5, and S_6. For the low-density setup of 32-electrode (Figure 6(b)), it can be observed that the proposed method also outperforms the other strategies since the precision of connectivity measure is increased by including temporal information to the estimated ROI time courses. As shown in (Lantz et al. 2003; Staljanssens et al. 2017), the performance of source connectivity analysis is affected by the number of electrodes. Therefore, the connectivity analysis improves for high-density setups. Figure 6(a,b) demonstrate that the appropriate inclusion of temporal stationarities improves the performance of source connectivity analysis and SOZ localization.

To evaluate the ability to determine the SOZ location, the minimum Euclidean distance between all dipoles belonging to the estimated SOZ and its actual simulated location is used as the criterion of performance. Figure 7 displays the criterion mean and its standard deviation after 100 trials for different SNR values in both EEG systems. Similar to MSE, the use of the dynamic estimation of ROIs time courses outperforms the other approaches. These results demonstrate that for the same ROIs, the mean Euclidean distance of determining the SOZ location depends on the strategy for estimating ROI

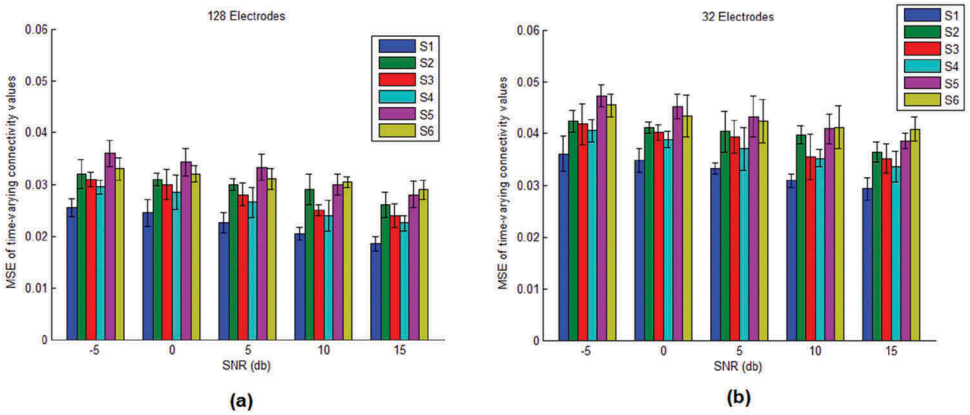

Figure 6. Performance of computer simulation; created with a BEM forward model. 100 repetitions are run with the simulated activity of three patch sources in different sizes. Each source includes non-stationary temporal dynamics of epileptic activities; see an example in Figure 1(a). Errorbars show the mean value and standard deviation of MSE between estimated and the ground truth time-varying connectivity values for different ROI time series estimation strategies under several SNR levels for 128-electrode EEG (a) and 32-electrode EEG (b) .

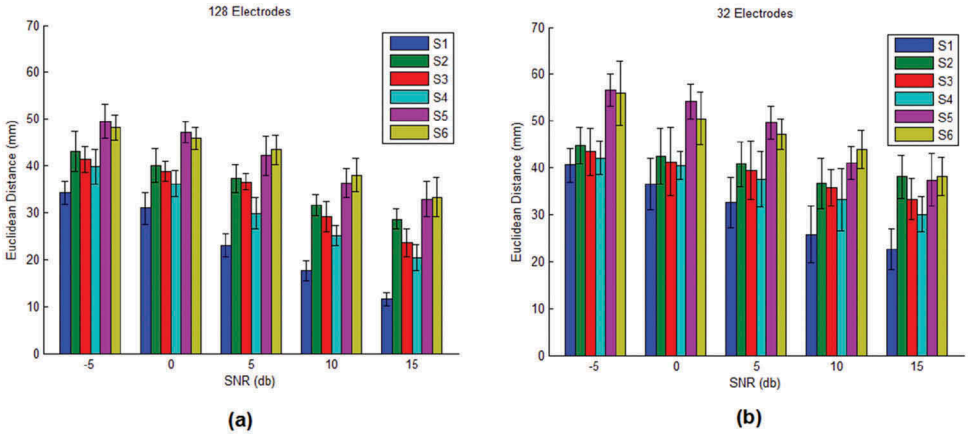

Figure 7. Performance of computer simulation; created with a BEM forward model. 100 repetitions are run with the simulated activity of three patch sources in different sizes. Each source includes non-stationary temporal dynamics of epileptic activities; see an example in Figure 1(a). Errorbars show the mean value and standard deviation of Euclidean distance of the SOZ location for different ROI time series estimation strategies under several SNR levels for 128- electrode EEG (a) and 32-electrode EEG (b).

time series. Among the aforementioned strategies, the proposed method uses temporal information for estimating cortical sources to improve the accuracy of SOZ localization. Thus, S_1 represents the best performance followed by S_4 and S_3. For 128-channel EEG, the mean Euclidean distance demonstrates that SOZ locations can be found accurately even in noisy conditions. Once again when the levels of SNR increases, estimation of SOZ location is improved, and as the result Euclidean distance decreases. Looking at 32-electrode EEG results (Figure 7(b)), S_1 also outperforms the other strategies since the quality of the computed ROIs time series strongly affects the accuracy of SOZ localization. It is observed that the Euclidean distance error increases as the number of EEG channels decreases, which means less spatial resolution. Also, for both EEG systems, the strategies of averaging over dipole time series (S_5) and using the resolution index (S_6) show the worst performance.

Real epilepsy dataset

For drugs-resistance epilepsy patients, surgery is an important treatment (Wiebe et al. 2001; De Tisi et al. 2011). Through epilepsy surgery, the region that causes the seizures is resected. To this end, one should successfully identify the brain region(s) that drive(s) seizures (Rosenow and Lüders 2001), called seizure onset zone (SOZ). On the other hand, the epileptogenic zone is a hypothetic zone due to its inability of being measured directly. One may use only the localization methods and find the regions with more activities, but it may lead to false zone. The main problem of this strategy

is that the epilepsy is a network disorder, i.e., during a seizure, several regions in brain become concurrently active as the parts of the epileptic network and usually it is difficult to decide which one(s) is/are the leading driver(s) of the network (Spencer 2002; Richardson 2012). In this paper, we estimate the SOZ using the proposed method. By means of source reconstruction and time-varying connectivity analysis, we can investigate the dynamics of the source signals and localize the epileptic driver, even it presents less activities.

Dataset description

In this work, we use the epilepsy dataset introduced in (Zwoliński et al. 2010). The original dataset includes EEG recordings of 23 patients of severe epilepsy diagnosed. EEG signals are recorded through the 10–20 system (with19 electrodes) using Ag/AgCl electrodes. In this paper, we use EEG recordings of only three of the patients. Table 1 shows the summary of the studied patient data.

Our analysis is focused on three epochs with epileptogenic structures, which are explicitly identified by the epileptologist. The epochs are preprocessed using common average referencing and band pass filtering between 0.5 Hz and 30 Hz. The forward problem is carried out in Fieldtrip, using the Colin 27 head (Holmes et al. 1998; Oostenveld et al. 2003). We also use the cortical surface provided by Fieldtrip for this anatomy with 8,000 vertices. To achieve the lead field matrix, a BEM head model consisting of three layers of brain, skull, and scalp with conductivities of 0.33 S/m, 0.015 S/m and 0.33 S/m, respectively (Oostendorp et al. 2000; Lai et al. 2005; Zhang et al. 2006).

In addition, a reference region is available to validate our results. This region is recognized as the structural location of the epileptogenic region marked by an expert on pre-surgical MRI scans in three projections; Moreover, this location is confirmed by ECoG and post-operational results.

Once the seizure is mapped and ictal ROIs are obtained, the time courses of the extracted ROIs, which are the input of ADTF analysis, are estimated. Next, the directed graph of outdegree values (which is calculated based on ADTF measures) is depicted. The ROI with the strongest relations (higher value of outdegree) is assigned as the location of SOZ, which drives the brain into ictal activity.

Table 1. Summary of the studied patient data.

Name	Gender	Age	Visual Inspection	Reference epileptic Zone
FRAANN	Female	17	Right frontotemporal repetitive synchronous spikes	Right temporal lobe
HRADAW	Male	12	Right repetitive synchronous frontotemporal spikes and bilateral frontotemporal ictal discharges	Right Frontal lobe
JANPRZ	Male	5	Right repetitive synchronous frontotemporal spikes	Right temporal lobe

Results

Fraann

Obtained localization result for subject FRAANN indicates activity primarily in the right temporal and frontal lobes (Figure 8(a)). This mapping corroborates the epileptologist description which is the right fronto-temporal region synchronization. Figure 8(b) shows the identified ROIs extracted from the former step. The numbers of identified ROIs are arranged from the highest power to the lowest power. It means that ROI 1 which is placed in the prefrontal region shows the highest power. Next is ROI 2, located in the inferior frontal region, and finally ROI 3 with the lowest power is mapped in the right middle temporal area.

Figure 9(a) displays the highest significant values $(\alpha = 0.01)$ of ADTF measures after using the surrogate data method. The x-axis demonstrates frequencies and the y–axis shows time samples. It can be seen that ROI 3 (temporal lobe) demonstrates more value in the time-frequency panel. Based on the Equation (4), for all pairs of ROIs, the directed graphs can be drawn as the model of the seizure propagation depicted in Figure 9(b). Solid arrows demonstrate stronger relations (higher values of outdegree), while dashed ones show weak interactions (lower values of outdegree).

Based on the directed graph of ADTF measures (Figure 9(b)), an irregular pattern can be observed during the seizure interval in the ROI 3 (right temporal region), while the most power full ROI is located in the prefrontal area (which may cause misleading estimation of SOZ location). Our finding agrees with the reference zone (right temporal lobe) which is validated by electrocorticography (ECoG) and post-operational results (Zwoliński et al. 2010)

Hradaw

The computed localization of subject HRADAW is presented in Figure 10(a). In this case, the reconstruction result demonstrates regions in the bilateral

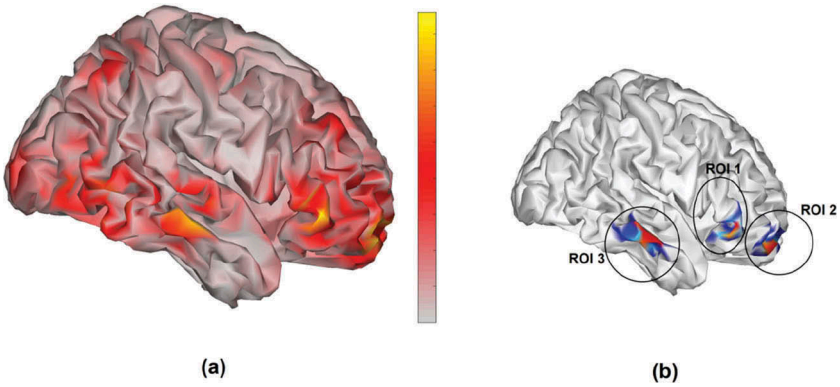

Figure 8. (a): Obtained localization result for subject FRAANN. The reconstruction result demonstrates regions in the right fronto-temporal region. (b): Identified ROIs from the localization step.

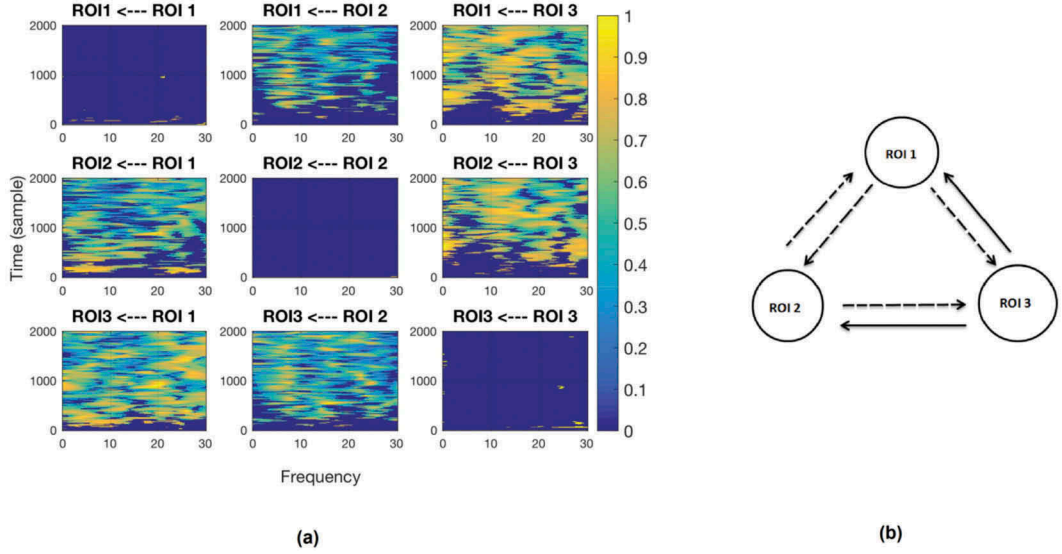

Figure 9. (a): The most significant values ($\alpha = 0.01$) of ADTF measures after using the surrogated data for subject FRAANN. The x-axis demonstrates frequencies and the y–axis shows time samples. (b): The directed graphs based on ADTF measures shows the seizure propagation. It illustrates unilateral strong relations in the ROI 3 (the lowest powerful ROI located in the right temporal region) during the seizure interval.

pre and central frontal lobe. However, the reference zone is found in the right frontal lobe. Using the reconstructed neural activity, the ROI sets of patient HRADAW are identified as shown in Figure 10(b). Four activated cortical locations (ROIs) are displayed over the topographic plots. The location of the most powerful ROI (ROI 1) is right prefrontal ROI and the rest of ROIs are placed in left prefrontal, right inferior frontal, and left inferior frontal regions, respectively.

The most significant values $(\alpha = 0.01)$ of ADTF measures are illustrated in Figure 11(a). The directed graph based on ADTF measures for subject HRADAW is depicted in Figure 11(b). It can be observed that significant direct interactions of ROI 1 flow to the other ROIs, i.e., ROI 1 acts as the origin of seizure.

Janprz

The obtained solution of subject JANPRZ is illustrated in Figure 12(a). In this case, the highest spatial peak of epileptic activity is placed in the right fronto-temporal region. This result agrees with the visual inspection of epileptologist and the

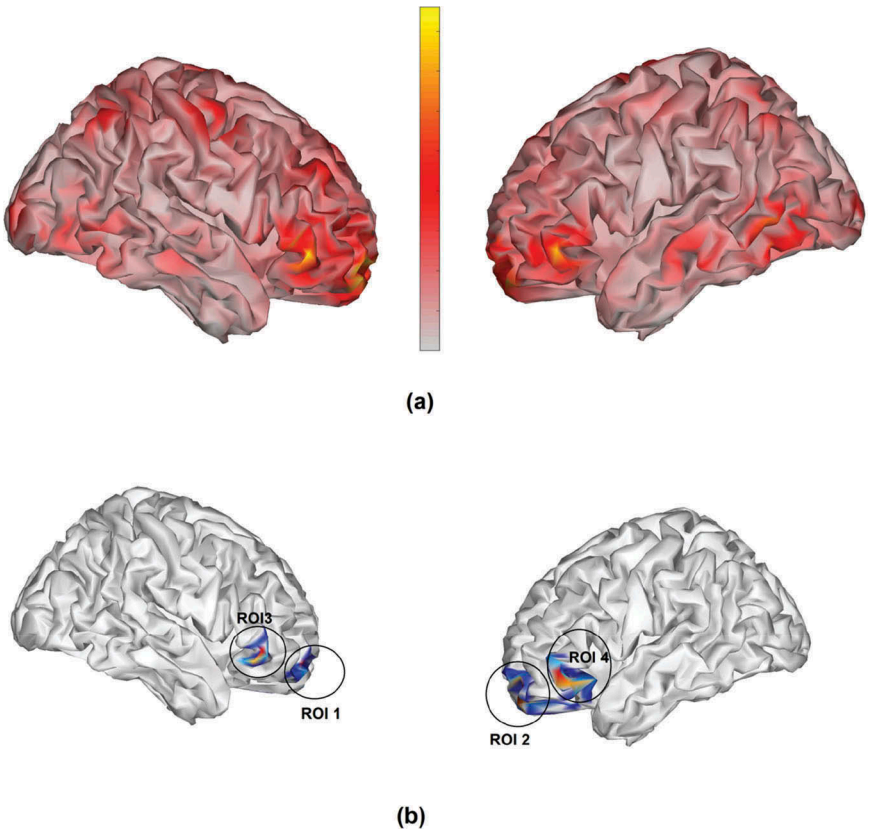

Figure 10. (a): Obtained localization result for subject HRADAW. The reconstruction result demonstrates regions in the bilateral pre and central frontal lobe. (b): Identified ROIs from localization step.

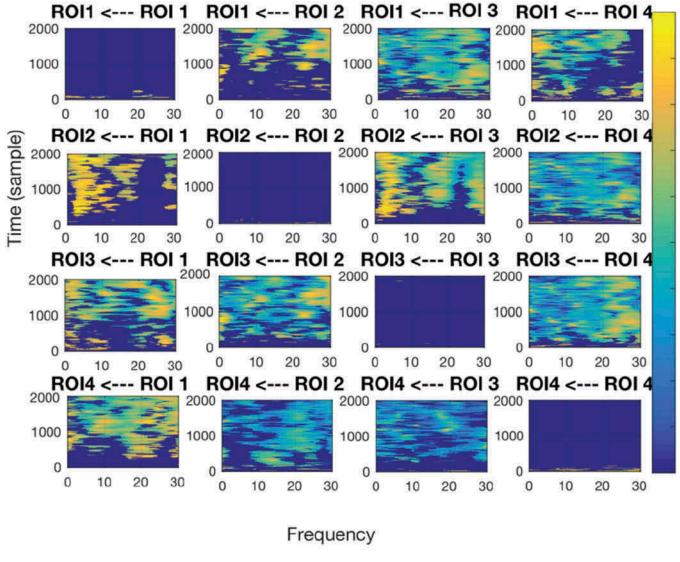

Figure 11. (a): The most significant values ($\alpha = 0.01$) of ADTF measures after using the surrogated data for subject HRADAW. The x-axis demonstrates frequencies and the y–axis shows time samples. (b): The directed graph based on ADTF measures shows the seizure propagation. It illustrates unilateral strong relations in the ROI 1 (the most powerful ROI located in the right prefrontal region) during the seizure interval.

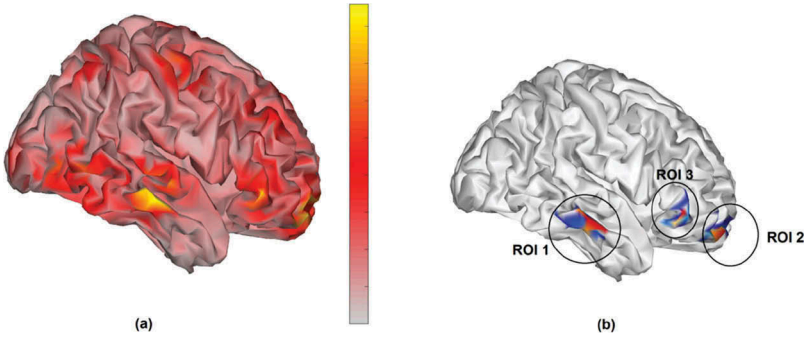

Figure 12. (a) Obtained localization result for subject JANPRZ. The highest spatial peak of activities is located in the right fronto-temporal region. This result agrees with the visual inspection of epileptologist. (b) Identified ROIs from localization step.

reference region. In details, the mapping discloses the powerful sources are placed in the right middle temporal gyrus, right prefrontal, and right inferior frontal areas. Among these ROIs, right middle temporal ROI (ROI 1) shows the highest spatial peak of activity (Figure 12(b)).

Figure 13(a) illustrates the most significant values $(\alpha = 0.01)$ of ADTF measures after using the surrogated data. Based on the Equation (4), for all pairs of ROIs, the directed graphs are calculated. Figure 13 (b) demonstrates two unilateral relationship (solid arrows) from the ROI 1 to the other ROIs which implies that this region is the location of SOZ.

The proposed method seems to present a better demonstration of the connectivity analysis between ROIs than the other strategies as it correctly finds the SOZ location based on referencing region, while the other strategies show at least a wrong detection. To keep the scope of the work narrow enough, we do not represent the results of the other strategies in the paper.

Discussion

We propose a new method that presents a time-varying source connectivity analysis using EEG signals. EEG signals have a high temporal resolution, but they suffer from low spatial resolution and volume conduction effect that cause false interactions. EEG source imaging (ESI) can solve both problems as it estimates the underlying sources that generate the recorded potentials (Hämäläinen and Ilmoniemi 1994; Pascual-Marqui et al. 1994; He et al. 2011, 2018b). The pipeline to obtain source connectivity from EEG data consists of three stages: (*i*) estimating of cortical sources (using source imaging methods); (*ii*) ROIs selection and time courses extractions; and (*iii*) estimating connectivity. Since the ROIs time series are the base of the further connectivity analysis, we focus on the second stage of the pipeline. For source connectivity analysis, at first, we estimate the cortical sources using LORETA.

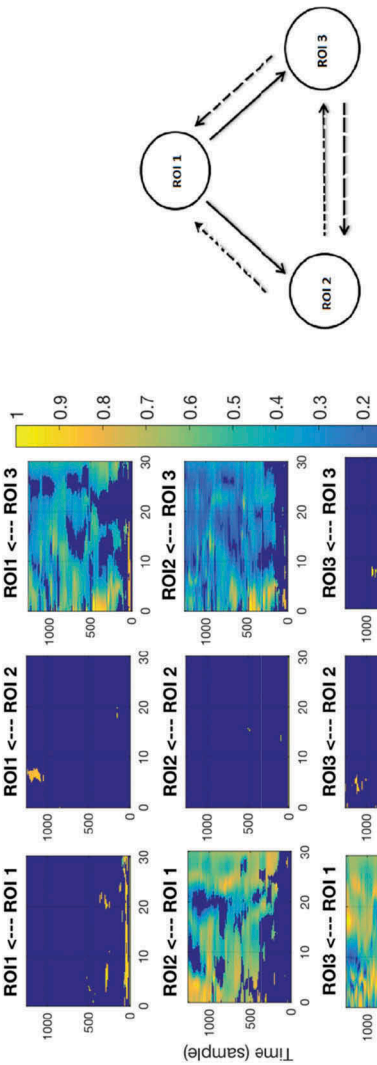

Figure 13. (a): The most significant values ($\alpha = 0.01$) of ADTF measures after using the surrogated data for subject JANPRZ. The x-axis demonstrates frequencies and the y–axis shows time samples. (b): The directed graphs based on ADTF measures shows the seizure propagation. It illustrates unilateral strong relations in the ROI 1 (the most powerful ROI located in the right temporal region) during the seizure interval.

The reconstructed source activity spreads over the whole cortical surface so it is necessary to identify spatially neighboring regions with high activity (the region of interest (ROI) set). The used ESI solution presents an appropriate seedpoint for the ROI determination process. Moreover, all ROIs should be assigned to the small and homogeneous clusters leading to a reliable connectivity analysis among networks. To this end, the ROIs are identified by scanning through the entire cortical surface to find the most activated dipoles and their neighboring regions. Then, we apply an approach that depends on the adjacent information from the EEG forward problem to find the active regions corresponding to the ground truth scenario (Friston et al. 2008). This strategy performs compact ROIs, which are more similar to reality. In this case, the estimated ROIs are appropriate for dealing with epileptic seizures. Especially when prior information about the localization of sources does not exists. In addition, the estimated areas are small and homogeneous, which improve connectivity calculation among networks.

While the quality of the estimated ROI time series extremely influences the connectivity analysis among ROIs, few strategies are introduced to estimate the activity inside each individual ROI. Usually, the time course of an ROI is derived by averaging the time courses through its dipoles (Hassan et al. 2014). However, each ROIs may encompass dipoles with different dynamics, thus the averaging may return a blurry or noisy time series demonstrating incorrect temporal behavior of that area. This problem would be worsen when Granger and phase based connectivity measures are calculated (Makeig et al. 2002; Ghumare et al. 2018). Another strategy is to choose the dipole with the maximum energy that does not correctly comprise the temporal dynamic of the entire region.

To address the aforementioned problems, we suggested a new method for ROI dynamics estimation as a single time course representing the time-variant information of each ROI. To this end, the brain activities are forced to come out only inside the regions of interest. Then, the ROI time series is estimated through a temporal penalty in the cost function that forces the temporal solution to be constant within a small temporal neighborhood but allows the temporal variations of neural brain activity over whole time horizon. This term makes the estimated time series follow smoothly non-stationarity of EEG signals and prevents the occurrence of abrupt changes in these signals.

The proposed approach is compared with different strategies for presenting ROI time series including time courses of the dipole with the maximum power (S_2) (Courellis et al. 2017), time series of the dipole with the highest singular value (S_3) (Sohrabpour et al. 2016), time course of the dipole with the maximum correlation with the averaged time series of the ROI (S_4) (Ghumare et al. 2018), the average of the estimated brain activity over the time courses of each ROI (S_5) (Hassan et al. 2014), and time course of the dipole with the nearest-to-one resolution index in the ROI (S_6) (Stenroos and Hauk 2013).

Effective brain connectivity discloses how the direction of information flows in the brain. Several methods are designed to measure the interactions between distant brain areas. Here, we used ADTF (Schlögl 2000; Omidvarnia et al. 2011), since its estimation of the connectivity has more reliable for the time-varying dynamics of the brain networks.

Estimating ROI time series is the most important step to correctly perform the source connectivity analysis since variations in connectivity patterns are directly related to how accurately the ROI time series are estimated. We compared the connectivity measure performance to evaluate the effect of time series extracted from each ROI.

We used simulated epileptic networks with a time-varying configuration to take the intrinsic non-stationary nature of EEG signals to account. A realistic head model is employed using the boundary element method and normal orientation of dipoles to the cortical surface. In our analysis, we added biological noise to the sources in order to simulate the background noise. Moreover, we added measurement noise with different variances.

For the real epileptic dataset, we study the epileptic network using the proposed method. For drug-resistance epilepsy patients, surgery is a key treatment option (Wiebe et al. 2001; De Tisi et al. 2011). To obtain successful epilepsy surgery, it is necessary to accurately find the SOZ localization. The proposed method is used to choose the ROI, which is more likely to generate the epileptic onset.

In the evaluation part, the MSE and correlation coefficient are employed to indicate differences between estimated ROI and ground truth time courses. On the other hand, MSE between the estimated and true time-varying connectivity values determines how well the ROI time series estimate their underlying networks. Finally, we objectively estimated network driver location and calculated the mean Euclidean distance for SOZ detection.

In summary, the proposed method (S_1), which is incorporating more precise estimation of the time series, involves the source dynamics and leads to the best source connectivity estimation. The second and third best strategies are S_4 (based on correlation with averaged time series) and S_3 (SVD-based selection). The resolution matrix-based strategy (S_6) and averaged-based strategy (S_5) presents the worst performance.

According to the estimated ROI time courses, we observe a lower MSE and higher correlation coefficients when S_1 strategy is used (Figures 4 and 5). Also, we observe an enhancement in the performance with increasing SNR levels. We consider the influence of the amount of EEG electrodes on the results. According to the literature (Michel and Murray 2012), the localization performance increases with the number of electrodes. This fact is illustrated by Figures 4 and 5, which are showing better performance for higher electrodes.

The comparison of time varying connectivity approach is performed using the aforementioned strategies. Interestingly, the MSE of the connectivity estimation obtained by the proposed approach is much lower compared to

the other strategies. The results also support our idea that for source connectivity studies, variations in connectivity patterns are highly related to the accurate estimation of the ROI time courses. Also, the MSE values decrease as levels of SNR increase (Figure 6). The proposed approach is the best one in the terms of SOZ detection accuracy in comparison with all other cases. Also, by increasing levels of SNR, an improvement in Euclidean distance values is observed (Figure 7). As shown in (Lantz et al. 2003; Staljanssens et al. 2017), the source connectivity performance is affected by the number of electrodes; Figures 6 and 7 confirm this effect. Our findings show that the appropriate inclusion of the non-stationarities can improve the performance of source connectivity analysis and SOZ localization.

We incorporate the proposed method to select the ROI that is more promising to generate the epileptic onset. The time series of each ROI is estimated dynamically for the next time-varying connectivity analysis. Then, a directed graph is calculated to find out which ROI demonstrates the most significant influence. Obtained results for real epileptic EEG data show that the proposed method performs well in finding SOZ location verified by ECoG and post-operational results. In some cases, the most powerful region is not epileptic region and the proposed method diagnoses the driver correctly which may be the less powerful region. The proposed ROI time series estimation directly affects the quality of connectivity analysis, since it shows better results (in selection the onset epileptic location) than the strategies that do not consider the dynamics of neural activity.

The performance of the involved localization method might decrease due to the several issues. Actually, an ESI method is harder to apply on epileptic activity due to non-stationarity nature of recordings. Also, several brain areas are simultaneously active, and they interact with each other. So a dynamic ESI method is required to encode the spatiotemporal neural dynamics of epileptic seizures. Moreover, appropriate preprocessing stage of the EEG recordings is needed to remove muscle and movement artifacts during seizures. For future works, a dynamic ESI method will be applied to encode the spatiotemporal neural dynamics of epileptic seizures. Also, both ROI identification and ROI time estimation strategies can be evaluated in a complete framework. Moreover, we will use the method for analyzing EEG recordings of emotional states or brain-computer interfaces.

Conclusion

In this article, we introduced a dynamic approach for estimating ROIs time courses from the reconstructed EEG sources. This approach explicitly includes the dynamics properties of brain activity in regions of interest. Simulation results indicated that the proposed method improves the accuracy

of extracted time series; and consequently the source connectivity analysis in comparison with the state-of-art methods. Also, time courses of the source with the highest correlation with averaged ROI time series and maximum singular value are acceptable alternatives. We used our method for finding SOZ location in drug-resistance epilepsy patients. The proposed ROI time series estimation directly affects the quality of connectivity analysis, leading to the best possible SOZ localization verified by ECoG and post-operational results. The choice between a pre-defined ROI definition and a data-driven ROI definition has an impact on performance.

Conflicts of interest

The author confirms that there are no known conflicts of interest associated with this publication.

Ethical approval

All procedures performed in studies involving human participants were in accordance with the ethical standards of the institutional and/or national research committee and with the 1964 Helsinki declaration and its later amendments or comparable ethical standards.

Funding

There has been no significant financial support for this work that could have influenced its outcome.

Informed consent

Informed consent was obtained from all individual participants included in the study.

Research involving animal rights

This article does not contain any studies with animals performed by any of the authors

ORCID

Karim Ansari-Asl http://orcid.org/0000-0003-1655-131X

References

Astolfi L, Cincotti F, Mattia D, Marciani MG, Baccala L, Fallani F, Salinari S, Ursino M, Zavaglia M, Babiloni F. 2006. Assessing cortical functional connectivity by partial directed coherence: simulations and application to real data. Biomed. Eng. IEEE Trans. 53 (9):1802–1812. doi: 10.1109/TBME.2006.873692.

Astolfi L, Cincotti F, Mattia D, Salinari S, Babiloni C, Basilisco A, Rossini PM, Ding L, Ni Y, He B. 2004. Estimation of the effective and functional human cortical connectivity with structural equation modeling and directed transfer function applied to high-resolution EEG. Magn Reson Imaging. 22(10):1457–1470. doi: 10.1016/j.mri.2004.10.006.

Brookes MJ, O'neill GC, Hall EL, Woolrich MW, Baker A, Corner SP, Robson SE, Morris PG, Barnes GR. 2014. Measuring temporal, spectral and spatial changes in electrophysiological brain network connectivity. Neuroimage. 91:282–299. doi: 10.1016/j.neuroimage.2013.12.066.

Campbell K, Kumar A, Hofman W. 1980. Human and automatic validation of a phase-locked loop spindle detection system. Electroencephalogr Clin Neurophysiol. 48(5):602–605.

Chella F, Marzetti L, Pizzella V, Zappasodi F, Nolte G. 2014. Third order spectral analysis robust to mixing artifacts for mapping cross-frequency interactions in EEG/MEG. Neuroimage. 91:146–161. doi: 10.1016/j.neuroimage.2013.12.064.

Comparison of different Kalman filter approaches in deriving time varying connectivity from EEG data. Engineering in Medicine and Biology Society (EMBC), 2015 37th Annual International Conference of the IEEE; 2015: IEEE.

Courellis H, Mullen T, Poizner H, Cauwenberghs G, Iversen JR. 2017. EEG-based quantification of cortical current density and dynamic causal connectivity generalized across subjects performing BCI-monitored cognitive tasks. Front Neurosci. 11:180. doi: 10.3389/fnins.2017.00180.

Da Silva FL. 2013. EEG and MEG: relevance to neuroscience. Neuron. 80(5):1112–1128. doi: 10.1016/j.neuron.2013.10.017.

Dale AM, Sereno MI. 1993. Improved localizadon of cortical activity by combining EEG and MEG with MRI cortical surface reconstruction: a linear approach. J Cogn Neurosci. 5 (2):162–176. doi: 10.1162/jocn.1993.5.2.162.

De Tisi J, Bell GS, Peacock JL, McEvoy AW, Harkness WF, Sander JW, Duncan JS. 2011. The long-term outcome of adult epilepsy surgery, patterns of seizure remission, and relapse: a cohort study. Lancet. 378(9800):1388–1395. doi: 10.1016/S0140-6736(11)60890-8.

Ding L, Worrell GA, Lagerlund TD, He B. 2007. Ictal source analysis: localization and imaging of causal interactions in humans. Neuroimage. 34(2):575–586. doi: 10.1016/j.neuroimage.2006.09.042.

Farahibozorg S-R, Henson RN, Hauk O. 2018. Adaptive cortical parcellations for source reconstructed EEG/MEG connectomes. Neuroimage. 169:23–45. doi: 10.1016/j.neuroimage.2017.09.009.

Fonov V, Evans AC, Botteron K, Almli CR, McKinstry RC, Collins DL, Brain Development Cooperative G. 2011. Unbiased average age-appropriate atlases for pediatric studies. Neuroimage. 54(1):313–327. doi: 10.1016/j.neuroimage.2010.07.033.

Friston K, Harrison L, Daunizeau J, Kiebel S, Phillips C, Trujillo-Barreto N, Henson R, Flandin G, Mattout J. 2008. Multiple sparse priors for the M/EEG inverse problem. Neuroimage. 39(3):1104–1120. doi: 10.1016/j.neuroimage.2007.09.048.

Ghumare EG, Schrooten M, Vandenberghe R, Dupont P. 2018. A Time-Varying Connectivity Analysis from Distributed EEG Sources: A Simulation Study. Brain Topogr. 31(5):1–17. doi: 10.1007/s10548-017-0616-5.

Giraldo-Suarez E, Martínez-Vargas JD, Castellanos-Dominguez G. 2016. Reconstruction of neural activity from EEG data using dynamic spatiotemporal constraints. Int J Neural Syst. 26(07):1650026. doi: 10.1142/S012906571650026X.

Grech R, Cassar T, Muscat J, Camilleri KP, Fabri SG, Zervakis M, Xanthopoulos P, Sakkalis V, Vanrumste B. 2008. Review on solving the inverse problem in EEG source analysis. J Neuroeng Rehabil. 5(1):25. doi: 10.1186/1743-0003-5-25.

Hämäläinen MS, Ilmoniemi RJ. 1994. Interpreting magnetic fields of the brain: minimum norm estimates. Med Biol Eng Comput. 32(1):35–42.

Hassan M, Dufor O, Merlet I, Berrou C, Wendling F. 2014. EEG source connectivity analysis: from dense array recordings to brain networks. PLoS One. 9(8):e105041. doi: 10.1371/journal.pone.0105041.

Hassan M, Merlet I, Mheich A, Kabbara A, Biraben A, Nica A, Wendling F. 2017. Identification of interictal epileptic networks from dense-EEG. Brain Topogr. 30 (1):60–76. doi: 10.1007/s10548-016-0517-z.

Hassan M, Wendling F. 2018. Electroencephalography source connectivity: aiming for high resolution of brain networks in time and space. IEEE Signal Process Mag. 35(3):81–96. doi: 10.1109/MSP.2017.2777518.

Haufe S, Nikulin VV, K-R M, Nolte G. 2013. A critical assessment of connectivity measures for EEG data: a simulation study. Neuroimage. 64:120–133. doi: 10.1016/j.neuroimage.2012.09.036.

Haufe S, Tomioka R, Dickhaus T, Sannelli C, Blankertz B, Nolte G, Müller K-R. 2011. Large-scale EEG/MEG source localization with spatial flexibility. Neuroimage. 54(2):851–859. doi: 10.1016/j.neuroimage.2010.09.003.

Hauk O, Wakeman DG, Henson R. 2011. Comparison of noise-normalized minimum norm estimates for MEG analysis using multiple resolution metrics. Neuroimage. 54 (3):1966–1974. doi: 10.1016/j.neuroimage.2010.09.053.

He B, Sohrabpour A, Brown E, Liu Z. 2018a. Electrophysiological source imaging: a noninvasive window to brain dynamics. Annu Rev Biomed Eng. doi: 10.1146/annurev-bioeng-062117-120853.

He B, Sohrabpour A, Brown E, Liu Z. 2018b. Electrophysiological source imaging: A noninvasive window to brain dynamics. Annu Rev Biomed Eng. 20:171–196. doi: 10.1146/annurev-bioeng-062117-120853.

He B, Yang L, Wilke C, Yuan H. 2011. Electrophysiological imaging of brain activity and connectivity—challenges and opportunities. Biomed. Eng. IEEE Trans. 58(7):1918–1931. doi: 10.1109/TBME.2011.2139210.

Holmes CJ, Hoge R, Collins L, Woods R, Toga AW, Evans AC. 1998. Enhancement of MR images using registration for signal averaging. J Comput Assist Tomogr. 22(2):324–333.

Kaminski M, Blinowska KJ. 1991. A new method of the description of the information flow in the brain structures. Biol Cybern. 65(3):203–210.

Lai Y, Van Drongelen W, Ding L, Hecox K, Towle V, Frim D, He B. 2005. Estimation of in vivo human brain-to-skull conductivity ratio from simultaneous extra-and intra-cranial electrical potential recordings. Clin Neurophysiol. 116(2):456–465. doi: 10.1016/j.clinph.2004.08.017.

Lantz G, De Peralta RG, Spinelli L, Seeck M, Michel C. 2003. Epileptic source localization with high density EEG: how many electrodes are needed? Clin Neurophysiol. 114(1):63–69.

Leistritz L, Schiecke K, Astolfi L, Witte H. 2016. Time-variant modeling of brain processes. Proc. IEEE. 104(2):262–281. doi: 10.1109/JPROC.2015.2497144.

Lie OV, van Mierlo P. 2017. Seizure-onset mapping based on time-variant multivariate functional connectivity analysis of high-dimensional intracranial EEG: a Kalman filter approach. Brain Topogr. 30(1):46–59. doi: 10.1007/s10548-016-0527-x.

Lu Y, Yang L, Worrell GA, He B. 2012. Seizure source imaging by means of FINE spatio-temporal dipole localization and directed transfer function in partial epilepsy patients. Clin Neurophysiol. 123(7):1275–1283. doi: 10.1016/j.clinph.2011.11.007.

Mahjoory K, Nikulin VV, Botrel L, Linkenkaer-Hansen K, Fato MM, Haufe S. 2017. Consistency of EEG source localization and connectivity estimates. Neuroimage. 152:590–601. doi: 10.1016/j.neuroimage.2017.02.076.

Makeig S, Westerfield M, Jung TP, Enghoff S, Townsend J, Courchesne E, Sejnowski TJ. 2002. Dynamic brain sources of visual evoked responses. Science. 295(5555):690–694. doi: 10.1126/science.1066168.

Martinez-Vargas JD, Strobbe G, Vonck K, van Mierlo P, Castellanos-Dominguez G. 2017. Improved localization of seizure onset zones using spatiotemporal constraints and time-varying source connectivity. Front Neurosci. 11:156. doi: 10.3389/fnins.2017.00156.

Mazziotta JC, Toga AW, Evans A, Fox P, Lancaster J. 1995. A probabilistic atlas of the human brain: theory and rationale for its development. The international consortium for brain mapping (ICBM). Neuroimage. 2(2):89–101.

Michel CM, Murray MM. 2012. Towards the utilization of EEG as a brain imaging tool. Neuroimage. 61(2):371–385. doi: 10.1016/j.neuroimage.2011.12.039.

Mosher JC, Leahy RM, Lewis PS. 1999. EEG and MEG: forward solutions for inverse methods. IEEE Trans Biomed Eng. 46(3):245–259.

Nolte G, Bai O, Wheaton L, Mari Z, Vorbach S, Hallett M. 2004. Identifying true brain interaction from EEG data using the imaginary part of coherency. Clin Neurophysiol. 115 (10):2292–2307. doi: 10.1016/j.clinph.2004.04.029.

Nunez PL, Srinivasan R, Westdorp AF, Wijesinghe RS, Tucker DM, Silberstein RB, Cadusch PJ. 1997. EEG coherency: I: statistics, reference electrode, volume conduction, Laplacians, cortical imaging, and interpretation at multiple scales. Electroencephalogr Clin Neurophysiol. 103(5):499–515.

Omidvarnia A, Mesbah M, O'Toole JM, Colditz PBoashash B. 2011. Analysis of the time-varying cortical neural connectivity in the newborn EEG: A time-frequency approach. International workshop on systems, signal processing and their applications, wosspa, tipaza, pp. 179–182. doi: 10.1109/WOSSPA.2011.5931445

Oostendorp TF, Delbeke J, Stegeman DF. 2000. The conductivity of the human skull: results of in vivo and in vitro measurements. IEEE Trans Biomed Eng. 47(11):1487–1492. doi: 10.1109/TBME.2000.880100.

Oostenveld R, Fries P, Maris E, Schoffelen J-M. 2011. FieldTrip: open source software for advanced analysis of MEG, EEG, and invasive electrophysiological data. Comput Intell Neurosci. 2011:1. doi: 10.1136/jnnp-2011-301944.

Oostenveld R, Stegeman DF, Praamstra P, van Oosterom A. 2003. Brain symmetry and topographic analysis of lateralized event-related potentials. Clin Neurophysiol. 114 (7):1194–1202.

Palus M, Hoyer D. 1998. Detecting nonlinearity and phase synchronization with surrogate data. IEEE Eng Med Biol Mag. 17(6):40–45.

Pascual-Marqui RD. 2002. Standardized low-resolution brain electromagnetic tomography (sLORETA): technical details. Methods Find Exp Clin Pharmacol. 24(SupplD):5–12.

Pascual-Marqui RD, Michel CM, Lehmann D. 1994. Low resolution electromagnetic tomography: a new method for localizing electrical activity in the brain. Int J Psychophysiol. 18 (1):49–65.

Pineda-Pardo JA, Bruña R, Woolrich M, Marcos A, Nobre AC, Maestú F, Vidaurre D. 2014. Guiding functional connectivity estimation by structural connectivity in MEG: an application to discrimination of conditions of mild cognitive impairment. Neuroimage. 101:765–777. doi: 10.1016/j.neuroimage.2014.08.002.

Rajabioun M, Nasrabadi AM, Shamsollahi MB. 2017. Estimation of effective brain connectivity with dual Kalman filter and EEG source localization methods. Australas Phys Eng Sci Med. 40(3):675–686. doi: 10.1007/s13246-017-0578-7.

Richardson MP. 2012. Large scale brain models of epilepsy: dynamics meets connectomics. J Neurol Neurosurg Psychiatry. jnnp-2011-301944. doi: 10.1136/jnnp-2011-301944.

Rosenow F, Lüders H. 2001. Presurgical evaluation of epilepsy. Brain. 124(9):1683–1700. doi: 10.1093/brain/124.9.1683.

Schlögl A. 2000. The electroencephalogram and the adaptive autoregressive model: theory and applications. Shaker Verlag GmbH, Aachen: Germany.

Schoffelen JM, Gross J. 2009. Source connectivity analysis with MEG and EEG. Hum Brain Mapp. 30(6):1857–1865. doi: 10.1002/hbm.20745.

Sohrabpour A, Ye S, Worrell GA, Zhang W, He B. 2016. Noninvasive electromagnetic source imaging and granger causality analysis: an electrophysiological Connectome (eConnectome) approach. IEEE Trans Biomed Eng. 63(12):2474–2487. doi: 10.1109/TBME.2016.2616474.

Spencer SS. 2002. Neural networks in human epilepsy: evidence of and implications for treatment. Epilepsia. 43(3):219–227.

Staljanssens W, Strobbe G, Van Holen R, Birot G, Gschwind M, Seeck M, Vandenberghe S, Vulliémoz S, van Mierlo P. 2017. Seizure onset zone localization from ictal high-density EEG in refractory focal epilepsy. Brain Topogr. 30(2):257–271. doi: 10.1007/s10548-016-0537-8.

Stenroos M, Hauk O. 2013. Minimum-norm cortical source estimation in layered head models is robust against skull conductivity error. Neuroimage. 81:265–272. doi: 10.1016/j.neuroimage.2013.04.086.

Theiler J, Eubank S, Longtin A, Galdrikian B, Farmer JD. 1992. Testing for nonlinearity in time series: the method of surrogate data. Physica D. 58(1–4):77–94. doi: 10.1016/0167-2789(92)90102-S.

Toppi J, Astolfi L, Poudel GR, Innes CR, Babiloni F, Jones RD. 2016. Time-varying effective connectivity of the cortical neuroelectric activity associated with behavioural microsleeps. Neuroimage. 124:421–432. doi: 10.1016/j.neuroimage.2015.08.059.

Valdes-Sosa PA, Roebroeck A, Daunizeau J, Friston K. 2011. Effective connectivity: influence, causality and biophysical modeling. Neuroimage. 58(2):339–361. doi: 10.1016/j.neuroimage.2011.03.058.

Van Mierlo P, Carrette E, Hallez H, Vonck K, Van Roost D, Boon P, Staelens S. 2011. Accurate epileptogenic focus localization through time-variant functional connectivity analysis of intracranial electroencephalographic signals. Neuroimage. 56(3):1122–1133. doi: 10.1016/j.neuroimage.2011.02.009.

van Mierlo P, Lie O, Staljanssens W, Coito A, Vulliémoz S. 2018. Influence of time-series normalization, number of nodes, connectivity and graph measure selection on seizure-onset zone localization from intracranial EEG. Brain Topogr. 5 (31) 753–766.

Wang Y, C-M T, Ombao H. 2016. Modeling effective connectivity in high-dimensional cortical source signals. IEEE J Sel Top Signal Process. 10(7):1315–1325. doi: 10.1109/JSTSP.2016.2600023.

Wiebe S, Blume WT, Girvin JP, Eliasziw M. 2001. A randomized, controlled trial of surgery for temporal-lobe epilepsy. N Engl J Med. 345(5):311–318. doi: 10.1056/NEJM200108023450501.

Wilke C, Ding L, He B. 2008. Estimation of time-varying connectivity patterns through the use of an adaptive directed transfer function. IEEE Trans Biomed Eng. 55(11):2557–2564. doi: 10.1109/TBME.2008.919885.

Wilke C, van Drongelen W, Kohrman M, He B. 2009. Identification of epileptogenic foci from causal analysis of ECoG interictal spike activity. Clin Neurophysiol. 120(8):1449–1456. doi: 10.1016/j.clinph.2009.04.024.

Zhang Y, Van Drongelen W, He B. 2006. Estimation of in vivo brain-to-skull conductivity ratio in humans. Appl Phys Lett. 89(22):223903. doi: 10.1063/1.2398883.

Zwoliński P, Roszkowski M, Żygierewicz J, Haufe S, Nolte G, Durka PJ. 2010. Open database of epileptic EEG with MRI and postoperational assessment of foci—a real world verification for the EEG inverse solutions. Neuroinformatics. 8(4):285–299. doi: 10.1007/s12021-010-9086-6.